Clinical Radiology 74 (2019) 489.e9–489.e15

Contents lists available at ScienceDirect

Clinical Radiology

journal homepage: www.clinicalradiologyonline.net

Magnetic resonance imaging assessment of the substrate for hyposmia in patients with Parkinson's disease

E.-J. Hwang [a,b,1], D.-W. Ryu [a,1], J.-E. Lee [a], S.-H. Park [b], H.-S. Choi [b,**], J.-S. Kim [a,*]

[a] Department of Neurology, College of Medicine, The Catholic University of Korea, Seoul, Republic of Korea
[b] Department of Radiology, College of Medicine, The Catholic University of Korea, Seoul, Republic of Korea

ARTICLE INFORMATION

Article history:
Received 30 September 2018
Accepted 6 February 2019

AIM: To assess whether multimodal magnetic resonance imaging (MRI) could detect neuroanatomical substrates that are distinctive to hyposmic Parkinson's disease (PD).

MATERIALS AND METHODS: Among 102 PD patients, 62 were hyposmic and 40 were normosmic. For each patient, a sagittal structural three-dimensional (3D) T1-weighted image was obtained with the magnetisation-prepared rapid acquisition of the gradient-echo sequence to generate subcortical grey matter masking templates and to perform a voxel-based morphometry analysis of the subcortical grey matter volumes. A 3D multi-echo gradient sequence was run to obtain axial magnitude and phase images to produce a quantitative susceptibility map (QSM), and a diffusion-weighted image was acquired to generate an apparent diffusion coefficient (ADC) map. The volumes and average QSM and ADC values of the 15 subcortical grey matter structures were calculated, and the group differences were evaluated using a one-way analysis of covariance with age and gender as covariates.

RESULTS: The QSM of the left thalamus significantly increased, while that of the right thalamus significantly decreased in hyposmia. No effects on the cortical volume changes were found other than aging.

CONCLUSION: The present results suggest that accumulation of disease-related substances in the left and right thalamus and the increasing asymmetry between the two sides are associated with hyposmia in PD.

Introduction

The olfactory system is composed of multiple neuronal connections between primary olfactory structures and the high-order cortex. The primary olfactory cortex, such as the anterior olfactory nucleus, lateral entorhinal cortex, amygdala, piriform cortex, and olfactory tubercles, receives afferent inputs from the peripheral olfactory bulbs. The medio-dorsal thalamic nucleus, which is associated with

* Guarantor and correspondent: J.-S. Kim, Department of Neurology, College of Medicine, The Catholic University of Korea, Seoul St. Mary's Hospital, 222, Banpo-daero, Seocho-gu, Seoul, 06591 Republic of Korea. Tel.: +82 2 2258 6078; fax: +82 2 599 9686.

** Guarantor and correspondent: H.-S. Choi, Department of Radiology, College of Medicine, The Catholic University of Korea, Seoul St. Mary's Hospital, 222, Banpo-daero, Seocho-gu, Seoul, 06591 Republic of Korea. Tel: +82 2 2258 6233; fax: +82 2 2258 6771.

E-mail addresses: hschoi@catholic.ac.kr (H.-S. Choi), neuronet@catholic.ac.kr (J.-S. Kim).

[1] These authors contributed equally to this work as the first author.

https://doi.org/10.1016/j.crad.2019.02.003
0009-9260/

alertness, mood, affection, sensory functions, memory, and cognition, transmits olfactory data from the primary olfactory cortex to the high-order prefrontal cortex.[1] Disruption in these networks causes olfactory dysfunction for odour detection, discrimination, and identification.

Hyposmia is relatively commonly found in the majority of Parkinson's disease (PD) patients and can precede the onset of motor symptoms by many years. Neuronal degeneration and α-synuclein pathology of the olfactory bulbs, the anterior olfactory nucleus, and the primary olfactory system in whole or in part may cause hyposmia. Although there is still some debate, olfactory dysfunction is usually non-progressive in nature from the start of the PD motor symptoms. In contrast to Alzheimer's disease, olfactory dysfunction manifests early in PD, and its pathology is detected in an olfactory bulb and nucleus.[2,3] Moreover, a recent study has revealed that normosmic PD had a benign clinical course and is a clinically distinct phenotype to hyposmic PD, and that the hyposmic PD patients had lower striatal dopamine transporter activities and more severe motor symptoms than normosmic PD patients.[4] Normosmic PD, which has lower pathological burden in the peripheral olfactory system than hyposmic PD, could be associated with a more benign disease process.

Although a number of pathological studies have been performed to characterise hyposmia in PD, an imaging methodology for assessing MRI substrates may provide another concept for understanding the disease process and help identify prospective PD patients with olfactory dysfunction. The hypothesis tested in the present study was whether multimodal magnetic resonance imaging (MRI) assessment could detect neuroanatomical substrates that are distinctive to hyposmic PD. Quantitative susceptibility mapping (QSM) is a novel imaging technique that helps determine bulk magnetic susceptibility distribution in tissues using gradient echo magnetic resonance phase images.[5] Apparent diffusion coefficient (ADC) mapping is a measure of the magnitude of water diffusion within tissues, which is calculated using MRI with diffusion-weighted imaging (DWI).[6] The present study evaluated the cortical and subcortical grey matter structures of PD patients using multimodal MRI techniques, including three-dimensional (3D) magnetisation-prepared rapid acquisition of gradient-echo (MPRAGE) images for volumetric measurements, QSM and ADC maps for magnetic susceptibility and diffusion estimation, respectively.

Materials and methods

Patients

The institutional review board approved the study protocol. Each patient provided informed consent for participation. A total of 102 patients between January 2015 and April 2016 were diagnosed with PD according to the UK brain bank criteria,[7] the presence of appropriate dopamine transporter defects on ^{18}F-N-(3-fluoropropyl)-2beta-carbon ethoxy-3beta-(4-iodophenyl) nortropane (FP-CIT) positron-emission tomography (PET), and the presence of PD drug response during the 12-month follow-up period. Clinical information including age, sex, disease duration, current medications, and history of arterial hypertension, diabetes mellitus, and cigarette smoking was collected. All patients were evaluated using the Unified Parkinson's Disease Rating Scale (UPDRS) and the modified Hoehn and Yahr (H&Y) stage. Patients (1) with dementia, (2) with neurological abnormalities related to atypical PD or secondary Parkinsonism, and (3) with history of psychiatric diagnosis and rhinological disorders, which can have a negative effect on olfaction, were excluded from the study.

Hyposmia was defined by the Cross-Cultural Smell Identification Test (CCSIT) result.[8] Before CCSIT, nasal problems that evoked olfactory dysfunction were checked by the otorhinolaryngological evaluation.

Cognitive function and dementia severity were evaluated with the Korean version of Mini Mental State Examination (K-MMSE), Global Deterioration Scale (GDS), and Seoul Neuropsychological Battery.[9]

Image acquisition

MRI images were acquired using a 3 T MR system (Magnetom Verio, Siemens, Erlangen, Germany) equipped with an eight-channel sensitivity encoding head coil. The sagittal structural 3D T1-weighted images were acquired with the MPRAGE sequence for image registration and volumetric measurement with the following acquisition parameters: repetition time (TR)=1,780 ms, echo time (TE)=2.2 ms, flip angle (FA)=9°, field-of-view (FOV)=256×256×256mm^3, acquisition voxel size=1×1×1mm^3. A fully first-order flow-compensated 3D multi-echo gradient-echo (GRE) sequence was used to acquire data for subsequent quantitative processing based on axial magnitude and phase images to create QSMs. The following parameters were used for image acquisition: TR=24 ms, TE=4.92, 7.38, 9.84, 12.3, 14.76, 17.22, and 19.68 ms, FA=15°, FOV=173×230×144 mm^3, and acquisition voxel size=0.72×0.72×2mm^3. Finally, the high-resolution DWI images with b-values of 0 and 1,000 s/mm^2 using readout-segmented echo planner imaging was acquired (TR=4,900 ms, TE=68 ms, FOV=220×220×156 mm^3, and acquisition voxel size=1.38×1.38×5 mm^3).

Subcortical grey matter segmentation using MPRAGE images

The subcortical grey matters were segmented on the MPRAGE images using FIRST, an automated segmentation and registration tool from the FMRIB Software Library (FSL; version 5.0, Functional Magnetic Resonance Imaging of the Brain Analysis Group, Oxford University, UK). After reorienting the sagittal MPRAGE images to match the orientation of the MNI152 standard template image, a total of 15 subcortical grey matter regions were extracted, including the accumbens, amygdala, caudate, hippocampus, pallidus, putamen, and thalamus of the left and right sides, and brainstem. Briefly, the images were initially registered to the MNI152 standard space template, and the inverse of this

transformation was performed in order to implement segmentation process. This software uses a Bayesian probabilistic model to search for the most probable shape of the subcortical structures of the input images, and the surface meshes of the subcortical structures are converted to boundary corrected volumetric representations. Once the successful segmentation for each input image was verified visually, the volumes of each region were normalised by a total intracranial volume of the same patient to compensate for different brain sizes among the patients.

QSM and ADC map generation

The magnitude and phase images acquired at multiple echoes from the 3D GE sequence were further processed using STI Suite software version 2.2, a MATLAB-based software package (MATLAB and Statistics Toolbox 2017b, The Mathworks, Inc., Natick, MA, USA) to produce QSMs. The software implemented a Lapacian-based phase unwrapping, a V-SHARP method, an improved version of the sophisticated harmonic artefact reduction (SHARP) method for background phase removal.[10] Removing background magnetic field contributions in MR phase images is an essential step for generating final QSMs. To perform SHARP, a spherical kernel radius and a regularisation parameter need to be defined. V-SHARP, on the other hand, uses different maximum radii for the spherical kernel and varying regularisation parameters to avoid dependence on MR acquisition and processing schemes.[11] The software also employed an iLSQR method to produce final QSMs, which iteratively removed streaking artefacts from the ill-conditioned *k*-space of an initial susceptibility map estimated by the least-squares-algorithm-based (LSQR) methods.[12] Furthermore, the ADC maps were generated by calculating mean diffusivity from the two different diffusion-weighted images acquired at b=0 and 1,000 s/mm^2.[13]

Co-registration of QSM and ADC maps into MPRAGE images

The QSM and ADC maps of the individual patients were co-registered to the MPRAGE images of the same patient using FLIRT, a FMRIB's linear affine image registration tool for brain images. This fully automated tool performs affine registration of an input image to a reference image by calculating an affine transformation matrix and by applying it to the input volume to be aligned with the reference volume. Once the successful registration of QSM and ADC to MPRAGE was achieved, the subcortical grey matter structures segmented from MPRAGE images were used as masking templates to extract subcortical structures from the QSM and ADC maps. The mean susceptibility in units of parts per billion (ppb) from QSM and ADC value in units of 10^{-6} mm^2/s from the 15 subcortical grey matter structures were calculated from the segmented structures.

Data analyses

All statistical analyses of clinical characteristics were calculated with a SPSS software version 24.0 for Windows (IBM Corporation, New York, NY, USA). Statistical significance was set at $p<0.05$. Patients with PD were subgrouped into hyposmic PD (CCSIT score <8) and normosmic PD (CCSIT score ≥8). Independent sample *t*-tests and analysis of covariance (ANCOVA) were used to compare group mean differences, and Pearson's χ^2 tests were used to compare frequencies for categorical variables.

Cortical grey matter analysis

The segmented cortical grey matter volumes of the MPRAGE images were analysed using FSL-VBM, an optimised voxel-based morphometry protocol executed with FSL software. Briefly, the cortical grey matter was segmented and registered to the MNI152 standard space template using non-linear registration. The MNI152 standard space template is the average of 152 normal T1-weighted structural MRI scans matched to the standard brain template created by the Montreal Neurological Institute (MNI). The study-specific grey matter template was created by averaging the individual grey matter images from the 40 hyposmic and 40 normosmic PD patients. All individual grey matter images were non-linearly registered to the study-specific template and were modulated to correct for local variations due to the non-linear component of the spatial transformation. The modulated cortical grey matter structures were smoothed with an isotopic Gaussian kernel with a sigma of 3 mm.

To investigate cortical grey matter differences between the hyposmic and normosmic PD groups, a general linear model was used to compare voxel-wise differences in cortical grey matter volumes. For each individual patient, a mean-centred age was added as a regressor to the model. Non-parametric statistics were performed with 5,000 permutations using a threshold free cluster enhancement option. The results were thresholded at $p<0.05$ with a family-wise error correction.

Subcortical grey matter analysis

The mean volumes (MPRAGE), mean susceptibility (QSM) and diffusion (ADC) values of the 15 subcortical grey matter structures of the hyposmic PD and normosmic PD groups were compared using one-way ANCOVA with age and gender as covariates with SPSS software. If the results indicated the presence of significant differences, a post hoc *t*-test with a Bonferroni correction was performed.

Results

Patients

Among the 102 PD patients, there were 62 patients with hyposmia (60.8%) and 40 with normosmia (39.2%). Mean CCSIT score of hyposmic patients was 5.2±1.6 and of normosmic patients was 8.9±1. Clinical characteristics of participants are summarised in Table 1. The clinical characteristics were not different between the two groups regarding sex, body mass index, disease duration, education years, a family history of PD, diabetes mellitus, hypertension,

or smoking habits. Motor signs measured by UPDRS, UPDRS sub-scores, and modified H&Y score, and cognitive scores measured by MMSE and GDS were not different between the two groups.

Cortical grey matter analysis results

No statistically significant voxel-wise differences in cortical grey matter volumes were found between hyposmia and normosmia with age as a covariate. Instead, the cortical grey matter atrophy was negatively associated with aging, and the decreased cortical volumes were found throughout the whole brain regions with increasing patients' ages (Electronic Supplementary Material Fig. S1).

Subcortical grey matter analysis results

Fig 1 illustrates representative slices of the MPRAGE, ADC, and QSMs of the normosmic and hyposmic PD patients, the segmented subcortical grey matter structures from MPRAGE in three different orientations, and Table 2 presents the mean, standard deviation, and ANCOVA results from the 15 subcortical grey matter structures measured by MPRAGE, QSM, and ADC. The hyposmic PD group showed relatively decreased volumes in most of the subcortical structures except for the left accumbens, left amygdala, and right putamen, but no statistically significant differences were discovered among the measured structures. The magnetic susceptibilities values in the majority of the hyposmic subcortical structures decreased, but those of the left hippocampus, left thalamus, right accumbens, and brainstem increased in hyposmia. The statistically significant differences between the two groups were also discovered in the left and right thalamus. Although the value was still negative, the QSM of the left thalamus increased in hyposmia, and the difference was statistically significant (F=4.316, p=0.045). For the right thalamus, the QSM decreased, and the difference was also statistically significant (F=4.232, p=0.047) between the two groups. It should also be noted that there was no statistically significant difference in thalamic QSM values between male and female groups. No significant relationship between gender and thalamic QSM was found within the normosmic group and the hyposmic group, separately, as well. Fig 2 illustrates the average and standard error of the mean QSM values of the normosmia and hyposmia groups. It is to be noted that a greater difference between the left and right thalami was found in the hyposmic PD group than in the normosmic PD group. Finally, the diffusion values in most of the hyposmic subcortical structures increased, except for the left and right hippocampus; however, no statistically significant differences between the two groups were found associated with diffusion.

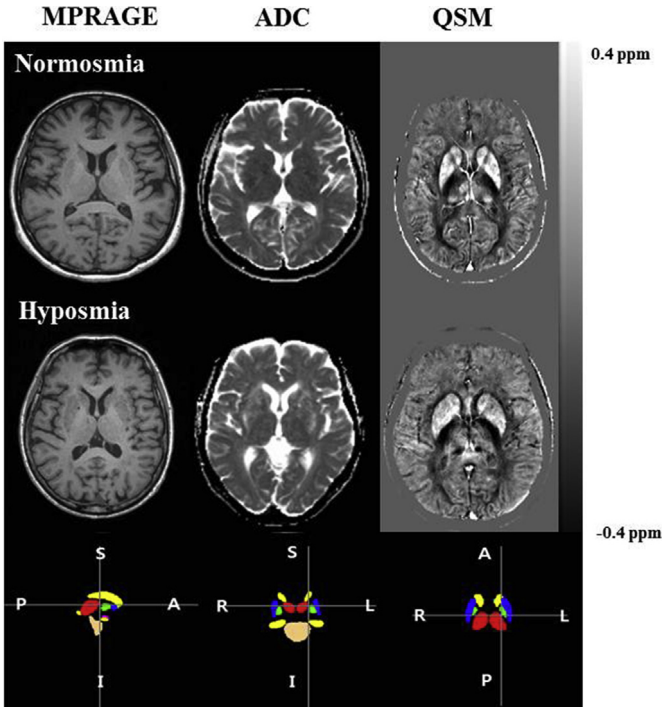

Figure 1 Representative slices of the MPRAGE images, ADC maps, and QSM of normosmia (top row), hyposmia PD patients (middle row) and representative images of the segmented deep grey matter regions in three different views. A=anterior, P=posterior, S=supine, I=inferior, R=right and L=left (bottom row).

Table 1
Clinical characteristics of patients.

	Hyposmia (n=62)	Normosmia (n=40)	p-Value
Age, year[a]	65.7±7.85	65.7±10.4	0.974
Male sex[b]	34 (54.8%)	14 (35.0%)	0.050
Body mass index (kg/m^2)[a]	23.4±3.0	23.6±3.5	0.786
Disease duration, year[a]	0.5±1.5	0.5±2.4	0.953
Education, year[a]	10.6±4.4	11±4.3	0.674
Family history of PD[b]	8 (12.9%)	6 (15.0%)	0.764
Hypertension[b]	23 (37.1%)	17 (42.5%)	0.585
Diabetes mellitus[b]	10 (16.1%)	6 (15.0%)	0.878
Current or ex-smoking[b]	17 (27.4%)	8 (20.0%)	0.395
UPDRS total[a]	26.2±14.5	25.6±15.9	0.835
UPDRS I[a]	2.1±1.9	2.2±1.8	0.797
UPDRS II[a]	7.2±4.3	7.8±7.0	0.619
UPDRS III[a]	16.8±10.8	15.7±8.6	0.574
H&Y score[a]	1.8±0.7	1.7±0.7	0.660
MMSE[c]	27±2.6	27.2±2.6	0.849
GDS[c]	2.7±0.7	2.5±0.8	0.131
CC-SIT[c]	5.2±1.6	8.9±1	<0.001

Values represent the mean±standard deviation and numbers of patients (percentage).
PD, Parkinson's disease; UPDRS, Unified Parkinson's Disease Rating Scale; H&Y, Hoehn & Yahr; MMSE, Mini Mental Status Examination; GDS, Global Deterioration Scale; CC-SIT, Cross-Cultural Smell Identification Test.
[a] Analyses were performed by independent sample t test.
[b] Analyses were performed by the chi-squared test.
[c] Analyses were performed by analysis of covariance controlling with age and education.

Discussion

The aim of the present study was to assess MRI substrates for hyposmia in PD using multimodal imaging techniques by evaluating the relative cortical grey matter volume changes, and the volumes, magnetic susceptibility, and diffusion of the subcortical grey matter structures using MPRAGE images, QSM, and ADC maps, respectively. This

Table 2
The mean, standard deviation, and analysis of co-variance results of the MPRAGE, QSM, and ADC differences between the normosmia and hyposmia PD groups.

MRI techniques (units)	structures	Normosmia	Hyposmia	F	*p*-Value
MPRAGE (normalised volume in %)	Lt accumbens	0.048±0.011	0.049±0.010	0.803	0.373
	Lt amygdala	0.141±0.020	0.142±0.024	0.201	0.646
	Lt caudate	0.309±0.026	0.300±0.024	1.741	0.229
	Lt hippocampus	0.340±0.048	0.337±0.048	0.096	0.757
	Lt pallidus	0.133±0.015	0.132±0.018	0.001	0.986
	Lt putamen	0.326±0.044	0.330±0.030	0.632	0.454
	Lt thalamus	0.546±0.051	0.531±0.049	0.776	0.390
	Rt accumbens	0.039±0.008	0.039±0.009	0.127	0.739
	Rt amygdala	0.140±0.015	0.138±0.019	0.045	0.834
	Rt caudate	0.315±0.030	0.313±0.026	0.035	0.857
	Rt hippocampus	0.358±0.042	0.351±0.040	0.004	0.954
	Rt pallidus	0.130±0.013	0.128±0.014	0.130	0.728
	Rt putamen	0.328±0.032	0.329±0.037	0.605	0.420
	Rt thalamus	0.530±0.047	0.516±0.050	0.696	0.411
	brainstem	1.840±0.177	1.810± 0.189	0.118	0.732
QSM (ppb)	Lt accumbens	0.0190±0.0282	0.0117±0.0410	0.846	0.314
	Lt amygdala	−0.0069±0.0097	−0.0069±0.0102	0.000	0.977
	Lt caudate	0.0298±0.0125	0.0255±0.0177	1.741	0.190
	Lt hippocampus	−0.0067±0.0081	−0.0054±0.0093	0.359	0.570
	Lt pallidus	0.0824±0.0494	0.0630±0.0571	3.001	0.074
	Lt putamen	0.0460±0.0193	0.0426±0.0237	1.333	0.177
	Lt thalamus	−0.0054±0.0081	−0.0017±0.0097	4.316	0.045
	Rt accumbens	0.0132±0.0366	0.0189±0.0349	0.427	0.515
	Rt amygdala	−0.0052±0.0098	−0.0071±0.0110	1.360	0.236
	Rt caudate	0.0298±0.0127	0.0249±0.0156	3.065	0.081
	Rt hippocampus	−0.0053±0.0086	−0.0085±0.0097	3.408	0.073
	Rt pallidus	0.0704±0.0462	0.0690±0.0483	0.138	0.715
	Rt putamen	0.0526±0.0244	0.0469±0.0272	1.478	0.213
	Rt thalamus	−0.0038±0.0080	−0.0069±0.0083	4.232	0.047
	brainstem	−0.0273±0.0114	−0.0231±0.0118	2.677	0.099
ADC (10^{-6} mm^2/s)	Lt accumbens	763.6±69.0	789±54.2	4.163	0.052
	Lt amygdala	915.9±90.9	939.7±95.3	1.268	0.245
	Lt caudate	1046.7± 128.1	1082.4±131.7	1.572	0.195
	Lt hippocampus	1022.3±148.7	1017.6±114.7	0.526	0.475
	Lt pallidus	693±56.3	696.6±59.6	0.030	0.883
	Lt putamen	680.9±40.1	692.2±60.2	0.983	0.344
	Lt thalamus	986.2±120.2	1016±116.5	1.051	0.306
	Rt accumbens	800.9±63.8	815.3±58.7	1.420	0.260
	Rt amygdala	959.9±105.9	966.7±89.0	0.055	0.842
	Rt caudate	1140.9±140.5	1177.2±177.4	0.948	0.296
	Rt hippocampus	1018.9±131.1	1018.1±118.8	0.334	0.564
	Rt pallidus	693±58.4	696.8±61.4	0.033	0.861
	Rt putamen	677.3±41.1	690.6±63.4	1.094	0.280
	Rt thalamus	991.3±117.7	1024.2±113.9	1.236	0.276
	brainstem	1123.8±130.8	1124±138.4	0.001	0.971

Values represent the mean±standard deviation.
MPRAGE, three-dimensional magnetisation-prepared rapid acquisition of gradient-echo; QSM, quantitative susceptibility map; ADC, apparent diffusion coefficient; PD, Parkinson's disease; MRI, Magnetic resonance imaging; ppb, parts per billion; Lt, left; Rt, right.

study revealed not only that the magnetic susceptibilities of the left and right thalamus in hyposmic PD changed significantly from those of the normosmic PD group, but also that the behaviours of the left and right sides were opposite; the magnetic susceptibility of the left thalamus increased, while that of the right thalamus decreased in hyposmia. Consequently, a greater asymmetry between the left and right sides was observed in the hyposmic thalamus. In relation to the prior knowledge that the thalamus relays olfactory sensory impulses from the peripheral receptors to cortical receptive areas,[1] the present findings suggest that accumulation of the disease-related substances in the left and right thalamus could contribute to the abnormal relaying of the sensory signals, leading to olfactory dysfunction in PD patients. Conversely, no effects on the cortical volume changes were found other than those of aging (Electronic Supplementary Material Fig. S1).

The significantly changed magnetic susceptibilities of the left and right thalamus in hyposmia suggest that olfactory dysfunction in PD patients could be associated with accumulation of the magnetic substances that are detectable to QSM. Magnetic susceptibility refers to tissue magnetisation that affects a main magnetic field inside MRI. Paramagnetic materials such as deoxyhaemoglobin, gadolinium-based contrast agents, irons and various metals are known to increase the local magnetic field and QSM values, while diamagnetic materials such as calcium and various types of proteins including α-synuclein are known to decrease the

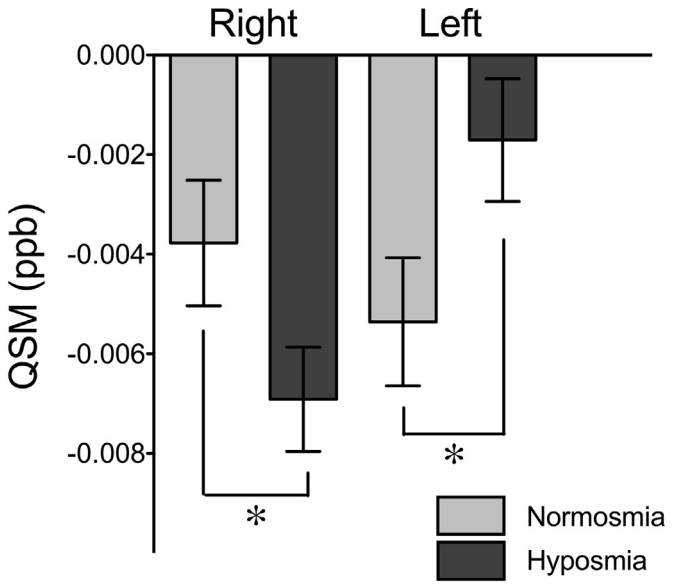

Figure 2 The average and standard error of the mean of the thalamic QSM values in the normosmia and hyposmia groups. The statistically significant differences were discovered in both left and right sides.

local magnetic field and QSM values.[14] Although the detailed mechanism is not known, the statistically significant changes in the hyposmic thalamus may infer the accretion of the disease-related substances associated with olfactory dysfunction in PD patients.

The increased asymmetry between the left and right thalamus in hyposmia as detected by QSM could be a characteristic of olfactory deficits in PD patients. In normosmic PD, the QSM values of the left and right thalamus were relatively similar; however, the magnetic susceptibility of the left thalamus significantly increased, while that of the right side significantly decreased in hyposmia (Fig 2). The present finding was consistent with the study reported by Zucco *et al.*, which claimed that unlike the age-matched healthy controls who showed no nostril-related differences, the patients with PD had poorer functioning of the left nostril and thus the olfactory deficit in PD was asymmetric.[15]

The thalamic asymmetry of hyposmia may also suggest separate roles of the left and right thalamus in olfactory function. The present results regarding the opposite behaviours of the left and right thalamus in hyposmia, support the previous study of Sela *et al.*, which reported that the right thalamus was associated with olfactomotor response processes such as olfactory discrimination, while the left side was related to olfactomotor control such as sniffing behaviours.[16] Given that our criterion for hyposmia was set on the CCSIT score, which measured the ability to discriminate various types of odours, it could be suggested that the diamagnetic shift of the right thalamus could identify hyposmia, while its left side was also changed in the opposite direction.

This study has several methodological strengths and limitations. Ages and cognitive status were matched between the two groups. Because olfactory dysfunction and the alternation of structural changes of MRI were associated with aging and cognitive status, the effects of aging and cognition on olfaction and the associated MRI changes could be excluded. There were several limitations. First, the odour identification in this study was measured by CCSIT instead of the 40-item University of Pennsylvania Smell Identification Test (UPSIT), which is widely used for assessment of the olfactory functions. Although CCSIT is less powerful to measure olfactory functions, it is more suitable for Asians who are less familiar with the items in UPSIT.[7] A larger number of patients and involvement of other ethnic groups should be considered in future studies to strengthen the results. Second, sex differences were not considered in this study. Olfactory impairment has been reported to be associated with sex and white/black races,[17] even though the differences were not confirmed in the Asian population. In this study, a greater male predominance was observed in the hyposmic group than in the normosmic group; however, the statistical tests showed no significant relationship between gender and the thalamic QSM values. Third, no age-matched healthy controls were involved in this study. Although the present results demonstrated the relative differences between normosmic and hyposmic PD, no reference point was provided to relate the present results to the behaviours of the healthy controls. The inclusion of age-matched controls would provide more information on hyposmic PD with respect to the controls.

In summary, the present study assessed the cortical grey matter volume changes and volumes, magnetic susceptibility and diffusion of the subcortical grey matter structures using multi-modal MRI techniques to examine the effects of olfactory dysfunction in PD patients. The association found between olfactory dysfunction and MRI abnormalities suggests that in patients with PD, the accumulations of disease-related materials in the left and right thalamus may lead to hyposmia in PD.

Conflict of interest

The authors declare no conflict of interest.

Acknowledgements

This research was supported by Basic Science Research Programme through the National Research Foundation of Korea funded by the Ministry of Science, ICT and Future Planning (NRF-2017R1D1A1B06028086).

Appendix A. Supplementary data

Supplementary data to this article can be found online at https://doi.org/10.1016/j.crad.2019.02.003.

References

1. Courtiol E, Wilson DA. The olfactory thalamus: unanswered questions about the role of the mediodorsal thalamic nucleus in olfaction. *Front Neural Circuits* 2015;**9**:49. https://doi.org/10.3389/fncir.2015.00049.
2. Doty RL. Olfactory dysfunction in Parkinson disease. *Nat Rev Neurol* 2012;**8**(6):329–39. https://doi.org/10.1038/nrneurol.2012.80.

3. Ruan Y, Zheng XY, Zhang HL, *et al*. Olfactory dysfunctions in neurodegenerative disorders. *J Neurosci Res* 2012;**90**(9):1693–700. https://doi.org/10.1002/jnr.23054.
4. Li DTH, Hui ES, Chan Q, *et al*. Quantitative susceptibility mapping as an indicator of subcortical and limbic iron abnormality in Parkinson's disease with dementia. *Neuroimage Clin* 2018;**20**:365–73. https://doi.org/10.1016/j.nicl.2018.07.028.
5. Takahashi H, Ishii K, Nashiwagi N, *et al*. Clinical application of apparent diffusion coefficient mapping in voxel-based morphometry in the diagnosis of Alzheimer's disease. *Clin Radiol* 2017;**72**:108–15. https://doi.org/10.1016/j.crad.2016.11.002.
6. Lee DH, Oh JS, Ham JH, *et al*. Is normosmic Parkinson disease a unique clinical phenotype? *Neurology* 2015;**85**(15):1270–5. https://doi.org/10.1212/WNL.0000000000001999.
7. Gibb WR, Lees AJ. The relevance of the Lewy body to the pathogenesis of idiopathic Parkinson's disease. *J Neurol Neurosurg Psychiatry* 1988;**51**(6):745–52.
8. Doty RL, Marcus A, Lee WW. Development of the 12-item Cross-Cultural Smell Identification Test (CC-SIT). *Laryngoscope* 1996;**106**(3):353–6.
9. Ahn HJ, Chin J, Park A, *et al*. Seoul Neuropsychological Screening Battery-dementia version (SNSB-D): a useful tool for assessing and monitoring cognitive impairments in dementia patients. *J Korean Med Sci* 2010;**25**(7):1071–6. https://doi.org/10.3346/jk ms.2010.25.7.1071.
10. Schweser F, Deistung A, Lehr BW, *et al*. Quantitative imaging of intrinsic magnetic tissue properties using MRI signal phase: an approach to *in vivo* brain iron metabolism? *Neuroimage* 2010;**54**(4):2789–807. https://doi.org/10.1016/j.neuroimage.2010.10.070.
11. Ozbay PS, Deistung A, Feng X, *et al*. A comprehensive numerical analysis of background phase correction with V-SHARP. *NMR Biomed* 2016;**30**:e3550. https://doi.org/10.1002/nbm.3550.
12. Li W, Wang N, Yu F, *et al*. A method for estimating and removing streaking artifacts in quantitative susceptibility mapping. *Neuroimage* 2015;**108**:111–22. https://doi.org/10.1016/j.neuroimage.2014.12.043.
13. Schaefer PW, Grant PE, Gonzalez RG. Diffusion-weighted MR imaging of the brain. *Radiology* 2000;**217**(2):331–45. https://doi.org/10.1148/radiology.217.2.r00ny24331.
14. Drescher M, Huber M, Subramaniam V. Hunting the chameleon: structural conformations of the intrinsically disordered protein alpha-synuclein. *Chembiochem* 2012;**13**(6):761–8. https://doi.org/10.1002/cbic.201200059.
15. Zucco GM, Rovatti F, Stevenson RJ. Olfactory asymmetric dysfunction in early Parkinson patients affected by unilateral disorder. *Front Psychol* 2015;**6**:1020. https://doi.org/10.3389/fpsyq.2015.01020.
16. Sela L, Sacher Y, Serfaty C, *et al*. Spared and impaired olfactory abilities after thalamic lesions. *J Neurosci* 2009;**29**(39):12059–69. https://doi.org/10.1523/JNEUROSCI.2114-09.2009.
17. Yaffe K, Freimer D, Chen H, *et al*. Olfaction and risk of dementia in a biracial cohort of older adults. *Neurology* 2017;**88**(5):456–62. https://doi.org/10.1212/WNL.0000000000003558.